The Eurasia Proceedings of Science, Technology, Engineering & Mathematics (EPSTEM)
ISSN: 2602-3199

The Eurasia Proceedings of Science, Technology, Engineering and Mathematics (EPSTEM), 2025

Volume 36, Pages 1-10

ICBAST 2025: International Conference on Basic Sciences and Technology

Epichlorohydrin-Crosslinked Nano-TiO_2/Plum Kernel Shell/Chitosan Hydrogel Beads for the Efficient Removal of Hexavalent Chromium from Aqueous Solutions

Serife Parlayici
Konya Technical University

Erol Pehlivan
Konya Technical University

Abstract: The removal of hexavalent chromium [Cr (VI)] from industrial wastewater remains a significant environmental challenge due to its extreme toxicity and serious risks to both human health and the ecosystem. This study aims to develop and evaluate a sustainable and efficient adsorbent for Cr (VI) removal from aqueous solutions. To achieve this, composite hydrogel beads composed of nano-TiO_2, plum kernel shell, and chitosan were synthesized using a sol-gel method and crosslinked with epichlorohydrin ($nTiO_2$–PKS–Cts@ECH). The morphological and structural characteristics of the biosorbent were analyzed using scanning electron microscopy (SEM) and Fourier-transform infrared spectroscopy (FTIR). Important operational factors, such as pH, adsorbent dose, contact time, and starting Cr (VI) concentration, were optimized using batch adsorption experiments. The equilibrium data were evaluated using the Langmuir, Freundlich, and Dubinin–Radushkevich isotherm models, with the Langmuir model showing the best fit, indicating monolayer adsorption and a maximum capacity of 97.09 mg/g. Kinetic analysis demonstrated that the adsorption process followed a pseudo-second-order model, suggesting that chemisorption, electrostatic attraction, and reduction collectively constitute the rate-limiting steps. Overall, the findings highlight the high potential of $nTiO_2$–PKS–Cts@ECH as a promising and eco-friendly biosorbent for the effective removal of Cr (VI) from contaminated water systems.

Keywords: Nano-TiO_2, Chitosan, Plum kernel shell, Epichlorohydrin, Chromium (VI)

Introduction

The high toxicity, mobility, and carcinogenic characteristics of heavy metals, especially hexavalent chromium [Cr (VI)], make them a serious hazard to human health and water quality (Mahmoud et al., 2022, Billah et al., 2022). Cr (VI), which is frequently released from processes like electroplating, leather tanning, and textile production, can remain in aquatic environments and build up in living things, having detrimental effects on the environment and biology. The development of economical and environmentally friendly alternatives is still a top environmental concern because traditional treatment techniques, including as chemical reduction, membrane filtration, and ion exchange, can have high operating costs, generate sludge, or have poor removal efficiency (Mahmoud et al., 2024.

Because of its porous structure, large surface area, and profusion of reactive functional groups including hydroxyl, carboxyl, and phenolic groups, the plum kernel shell's structure is crucial to its effectiveness in eliminating Cr (VI) from aqueous solutions. Shell part of the plum seed consists mainly of carbon and oxygen represents the elemental composition characteristic of organic substances, since they are the main components of organic molecules (Usmonova and Salixanova, 2025). Strong adsorption interactions with Cr (VI) ions are made possible by these structural characteristics via surface complexation, ion exchange, and electrostatic

- This is an Open Access article distributed under the terms of the Creative Commons Attribution-Noncommercial 4.0 Unported License, permitting all non-commercial use, distribution, and reproduction in any medium, provided the original work is properly cited.

- Selection and peer-review under responsibility of the Organizing Committee of the Conference

© 2025 Published by ISRES Publishing: www.isres.org

attraction. Its mechanical stability and chemical reactivity are also improved by the shell's lignocellulosic composition, which is mostly composed of cellulose, hemicellulose, and lignin. This allows for activation or modification to further increase the shell's adsorption capacity. For the treatment of water contaminated with toxic Cr (VI), this low-cost, renewable, and natural biomass provides an effective and environmentally friendly alternative.

Chitosan, a naturally occurring biopolymer formed from chitin, has drawn interest among other biosorbents due to its abundance of functional groups (such as -OH and -NH_2) that aid in metal ion binding, as well as its biodegradability and biocompatibility (Jiménez-Gómez & Cecilia, 2020). Chitosan, a naturally occurring biopolymer, is useful in many fields, including environmental protection and healthcare (Al-Obaidi, 2023 etal., 2023; Alsuhaibani et al., 2024, Ke et al., 2021). However, the actual use of native chitosan is limited by its mechanical constraints, which include low stability and solubility in acidic environments. Crosslinking with substances like epichlorohydrin and adding inorganic and bio-based fillers have been investigated as ways to improve the structural integrity and adsorption effectiveness of chitosan in order to get around these drawbacks. As a powerful crosslinking agent that improves the structural integrity and functional performance of composite materials, epichlorohydrin is essential to the creation of sophisticated hydrogel-based adsorbents. Epichlorohydrin crosslinks chitosan with nano-TiO_2 particles and plum kernel shell biomass to help create a stable three-dimensional polymeric network. Crosslinking chitosan with epichlorohydrin expands the spacing between chitosan chains, which enhances the rate of adsorption, even when the material is in a dry state (Rocher et al., 2010). The hydrogel beads' mechanical strength and chemical durability are increased by this crosslinking, which also helps to create a porous matrix with improved adsorption capacity and active site accessibility.

The combination of nanomaterials with biopolymers has created new avenues for the creation of high-performing hybrid adsorbents in recent years. In environmental applications, nano-TiO_2—which is well-known for its photocatalytic activity, thermal stability, and wide surface area—has shown beneficial benefits when paired with biopolymer matrices. Nano-TiO_2 with biomaterial can effectively degrade persistent organic pollutants that are resistant to biodegradation (Guo et al., 2025). The adsorption capabilities of the hybrid system are further improved by the availability and affordability of porous carbonaceous material from agricultural by-products like plum kernel shell (PKS), which has a high lignocellulosic content. A highly efficient adsorbent for the removal of Cr (VI) may be produced by combining these elements into a single, functionalized composite.

This study focuses on creating and testing new hydrogel beads made from a composite of titanium dioxide nanoparticles, plum kernel shells, and chitosan, which are crosslinked with epichlorohydrin. The purpose of these beads is to act as a versatile adsorbent for removing Cr (VI) from water. Researchers developed the composite beads to combine the unique properties of each ingredient. They then conducted experiments to see how factors like pH, contact time, initial Cr (VI) concentration, and the amount of adsorbent used affected how well the nano-composite beads removed the Cr (VI). The results suggest that these hybrid hydrogel beads are a promising, effective, and eco-friendly option for cleaning up water contaminated with Cr (VI).

Results and Discussion

Materials and Experimentation

The supplier of the chitosan (degree of deacetylation, DD=75–85%) was Sigma-Aldrich. The acetic acid (CH_3COOH, >99 % purity), HCl, NaOH and $K_2Cr_2O_7$ salt (purity: ≥99.9 %) were provided by the Merck Company. TiO_2 nano-particles were obtained from Sigma-Aldrich (St Louis, MO, USA). The epichlorohydrin (ECH) cross-linker was obtained from Merck (Darmstadt, Germany). All relevant chemicals used in the experiments were of analytical grade. Plum kernels were collected from an orchard near Konya, Türkiye, and their shells were used in the synthesis of adsorbents. In the preparation of the composite adsorbent, an IKAMAG-RO15 model mechanical stirrer, a GFL 3033 model thermostatic shaker, and a pH meter with glass electrodes (Orion 900S2) were used. A UV-visible spectrophotometer (Schmadzu UV-1700) was used for the determination of MB (λmax: 664 nm). The FT-IR spectrum was recorded on a Bruker VERTEX 70 FT-IR spectrometer. The microstructure of the adsorbent was examined using scanning electron microscopy (SEM, Nova Nano SEM 200, FEI Company).

Preparation of Raw Material

Plum kernels were separated from the fruit, the they were cleaned of dirt, washed, and dried. The dried kernels were first ground into powder using a mill and sieved to a particle size of 125 µm. The powdered kernel shells were then washed several times with 0.1 mol L^{-1} HCl, followed by several times with distilled water, and dried at room temperature for 24 hours. This prepared PKS powder was used in composite synthesis.

Synthesis of Adsorbent

The preparation process of $nTiO_2$–PKS–Cts@ECH is shown in Figure 1. A viscous gel was prepared by dissolving 3 g of chitosan in 300 mL of acetic acid (0.1 mol L^{-1}) solution. Then, 1.5 g of PKS and 1.5 g of $nTiO_2$ were added to the homogenate gel and stirred at room temperature for 12 h. The mixed solution was slowly dropped into a precipitation bath containing 200 mL of 5% NaOH and 300 mL of 6% ethyl alcohol to form small beads and left to stand for 24 h. The beads were filtered and washed several times with deionized water until the pH of the solution phase became neutral. The beads were cross-linked in 1% ECH solution at 50 °C for 6 h. After the reaction, the composite spheres were filtered and rinsed repeatedly with deionized water, then allowed to dry for 24 h and stored until use.

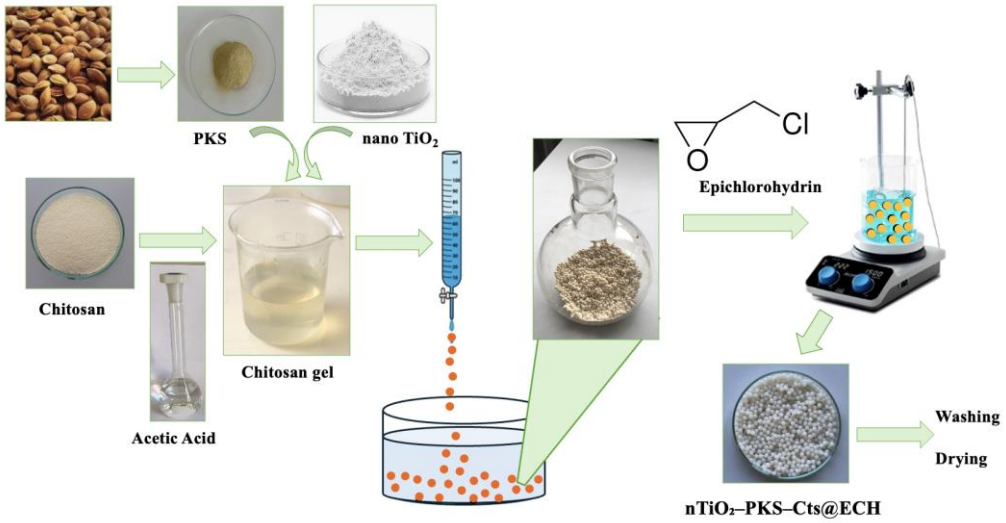

Figure 1. Schematic steps of $nTiO_2$–PKS–Cts@ECH beads synthesis

Batch Adsorption Experiments

To evaluate the adsorption efficiency of Cr (VI) removal from aqueous solutions using $nTiO_2$–PKS–Cts@ECH beads, batch adsorption experiments were conducted. First, a Cr (VI) stock solution was prepared by weighing 2.83 g of $K_2Cr_2O_7$ (≥99.0%) and dissolving it in distilled water to 1000 mg/L (Masuku et al., 2024). Subsequent dilutions with distilled water were performed to reach the desired initial Cr (VI) concentration for the adsorption tests. To determine the effect of various parameters on the adsorption efficiency and capacity of $nTiO_2$–PKS–Cts@ECH beads, experiments were systematically conducted using varying factors such as solution pH, initial concentration, adsorbent dosage, temperature, and contact time. For this purpose, pH (2, 3, 4, 5, 6, 7, 8, and 9), dye initial concentration (10, 25, 50, 75, 100, 150, 200, 250, 400, and 500 mg L^{-1}), adsorbent dosage (0.5, 1.0, 1.5, 2.0, 3.0, and 4 g L^{-1}), contact time (5, 15, 30, 45, 60, 90, 120, 180, 240, 300, and 360 min) and temperature (25, 35, 45, and 55 °C) parameters were optimized. The composite beads were mixed with Cr (VI) solutions of known concentrations under regulated conditions. Cr (VI) ions remain in the solution after the adsorption process were determined by UV-Vis spectrophotometry by analyzing the beads at regular intervals after filtration. Changes between the initial and final Cr (VI) concentrations were used to calculate the adsorption capacity (q_e, mg/g) and removal efficiency (%).

$$q_e = \frac{C_{0,Cr(VI)} - C_{e,Cr(VI)}}{m} V \quad (1)$$

$$Removal\ (\%) = \frac{C_{0,Cr(VI)} - C_{e,Cr(VI)}}{C_{0,Cr(VI)}} 100 \quad (2)$$

Structural and Morphological Characterization of the Nano-Composites

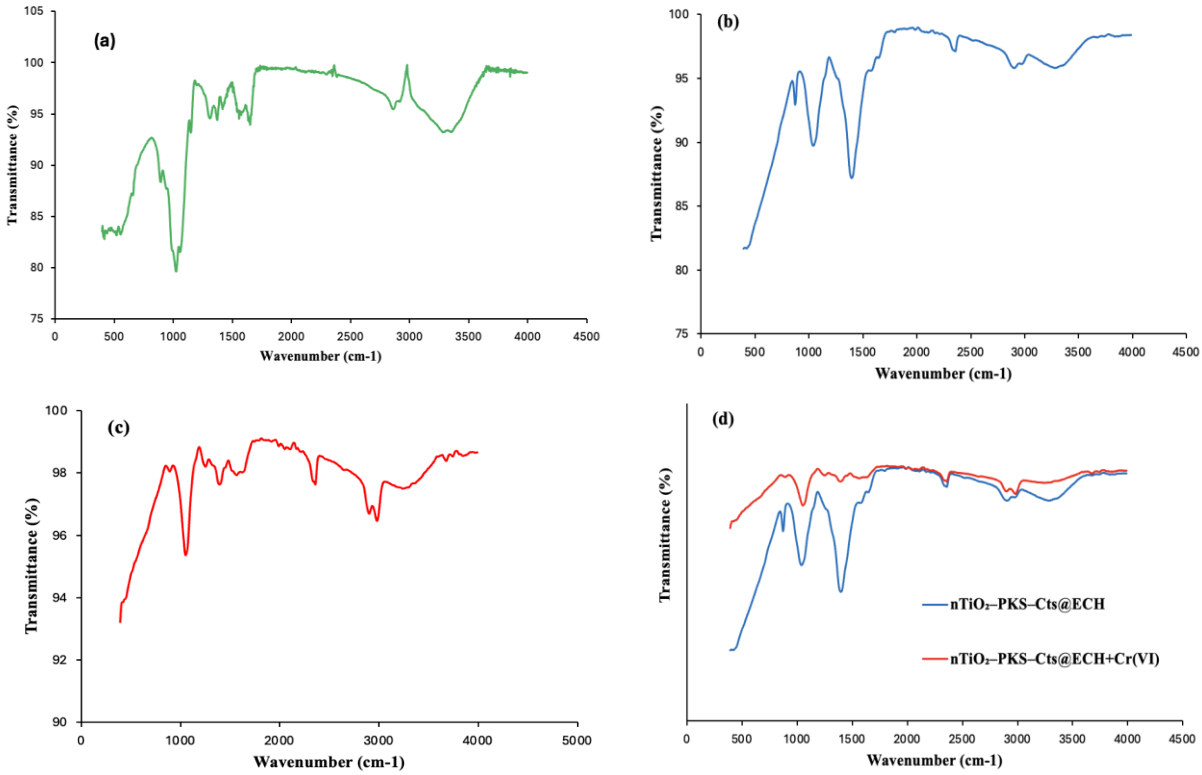

Figure 2. FT-IR diagram of chitosan (a), nTiO₂–PKS–Cts@ECH (b), nTiO₂–PKS–Cts@ECH+ Cr (VI) (c) and comparison of Cr (VI) adsorption before and after (d)

Figure 2(a-d) shows the FT-IR spectra of chitosan, nTiO₂–PKS–Cts@ECH, nTiO₂–PKS–Cts@ECH, and the composite before and after Cr (VI) adsorption. FT-IR analysis identifies key functional groups, providing insight into the molecular interactions within the nTiO₂–PKS–Cts@ECH structure and highlighting potential active sites responsible for Cr (VI) ion adsorption. N-H and O-H groups in chitosan are also observed around 3350 cm-1 (Khan et al. 2024). In addition, the absorption bands at 2919 and 2867 cm-1 can be attributed to C-H symmetric and asymmetric stretching, respectively (Teshome et al., 2024).

The amide II peak in chitosan is observed at 1560 cm-1 and 1375 cm-1, and characteristic peaks belonging to NHCOCH3 stretching are observed. The absorption band at 1026 cm-1 is due to the symmetric stretching of C-O-C bonds (Parlayıcı & Pehlivan, 2024). These bands are characteristics typical of polysaccharide and are found in other polysaccharide spectra, such as xylan, glucans and carrageenans. These features confirm that Cht is rich in amino groups, which play a crucial role in its adsorption capabilities. When the spectrum of nTiO₂–PKS–Cts@ECH was examined (Figure 2b), the peaks around 3371 and 3278 cm-1 belonged to hydroxyl and amino groups, respectively. Smaller peaks included the peak at 2865 cm-1 matching C-H bonds, the peak at 1646 cm-1 generally seen in type I amides, and the peak at 1582 cm-1 associated with type II amide groups. The peaks appearing at 1425 and 1375 cm-1 represented CH3N-acetylglucosamine and -CH2 groups, respectively. The peaks at 1068 and 1026 cm-1 indicated the presence of C-O bonds. The peak of the C-O vibration indicated the presence of hemicellulose in the biosorbent. Oxygen in TiO2 was observed at 1090–1200 cm-1 and the band at 500 cm-1 was due to Ti-O vibrations.

In the figure, the FT-IR spectrum of nTiO₂–PKS–Cts@ECH before adsorption was compared with the spectrum of nTiO₂–PKS–Cts@ECH after Cr (VI) adsorption. When the spectra before and after the adsorption of Cr (VI) were compared (Figure 2d), differences in the positions and peak intensities of the absorbance peaks were revealed. After the adsorption of Cr (VI), the asymmetric stretching vibration at 3371 cm-1 was significantly disrupted, suggesting that chemical interactions occurred between Cr (VI) ions and hydroxyl groups on the nTiO₂–PKS–Cts@ECH surface. The peak observed at 1375 cm-1 before adsorption shifted to 1396 cm-1 after Cr (VI) adsorption, and the peak intensity became smaller. Slight shifts and distortions in the C–O band (1068 to 1026 cm-1) and the amine (N–H) band (3278 cm-1) were observed. FT-IR post-adsorption spectra indicate that functional groups play a role in the adsorption processes.

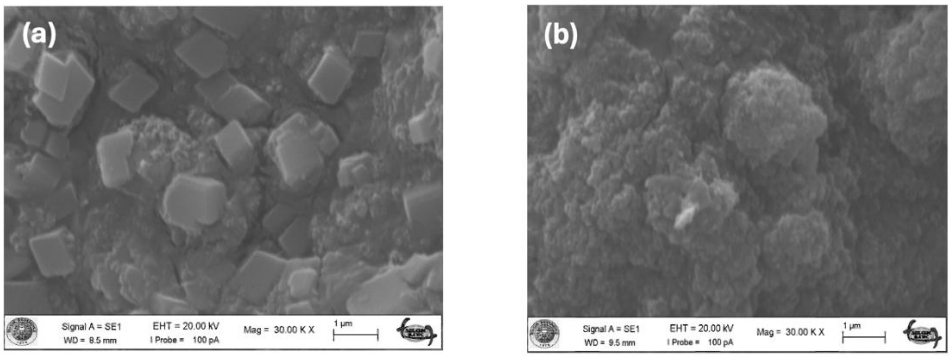

Figure 3. SEM image of (a) nTiO₂–PKS–Cts@ECH before MB adsorption (b) nTiO₂–PKS–Cts@ECH composite after MB adsorption

SEM was used to study the surface of the nTiO₂–PKS–Cts@ECH composite. The images in Figure 3a show the original, porous structure of the composite before it was used to treat Cr (VI). After the composite was used to adsorb Cr (VI) ions, the SEM images in Figure 3b clearly show that the surface became more homogenous and saturated. This visual change indicates that the pores and active sites on the adsorbent's surface have been successfully occupied by the Cr (VI) ions.

Results of the Batch Adsorption Experiments

Effect of nTiO₂–PKS–Cts@ECH Dosage

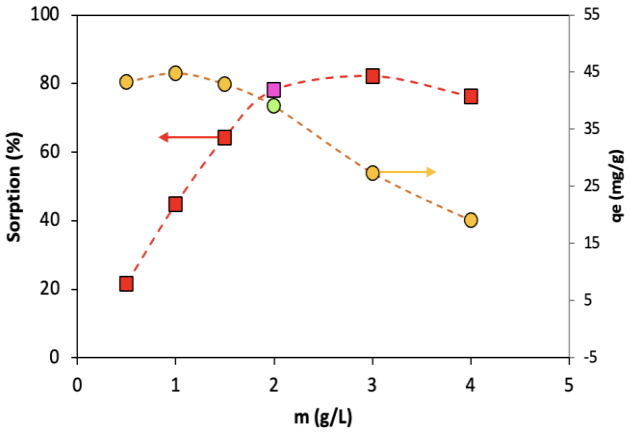

Figure 4. Effect of nTiO₂–PKS–Cts@ECH composite dosage

The amount of Cr (VI) retention was examined by adsorption experiments at different adsorbent doses (0.5, 1.0, 1.5, 2.0 , 3.0 and 4.0 g/L). In Figure 4, the adsorption capacities and sorption% values are plotted against the varying amount of adsorbent. Generally, as the adsorbent dose increases, the Cr (VI) retention capacity of the adsorbent first increases to a certain value and then decreases. At the same time sorption % increased up to this value again and after the dose was increased then it reached a stable value. In case the amount of nTiO₂–PKS–Cts@ECH increases from 0.5.0-2.0 g/L, the adsorption is increased quickly for the Cr (VI). After 2.0 g/L of nTiO₂–PKS–Cts@ECH dosages, it was observed that the adsorption remained stationary and small increment in the adsorption value was obtained. The capacity of adsorbent increased proportional to the adsorbent dose until 2.0 g/L.

Effect of pH

The effectiveness of the nTiO₂–PKS–Cts@ECH beads in removing Cr (VI) is largely dependent on the pH of the aqueous solution. Cr (VI) is mostly found as $HCrO_4^-$ and $Cr_2O_7^{2-}$ ions at lower pH values (Zewde et al., 2024; Nishad et al., 2025), especially in the acidic range (usually around pH 2–4). pH values at different values (2, 3, 4, 5, 6, 7, 8, 9) were tried in the solution phase for the adsorption of Cr (VI). From the figure, it is observed that the adsorption capacity decreases as the pH increases. These ions are more easily adsorbed onto

the protonated surface of the hydrogel beads because of increased electrostatic attraction. With its many amino groups, the chitosan component gets highly protonated in acidic environments, which raises the positive surface charge and enhances its ability to interact with negatively charged Cr (VI) species. Further aiding elimination, the TiO_2 nanoparticles might also help reduce Cr (VI) to some extent. On the other hand, the removal efficiency tends to drastically decline when the pH rises toward neutral or alkaline conditions.Functional groups on the adsorbent surface deprotonate, which lowers the electrostatic interaction between the adsorbent and anionic Cr (VI) species. At higher pH, these species also start to transition toward the CrO_4^{2-} form. Furthermore, chromate species and hydroxide ions may compete more for active sites at higher pH values, which would further inhibit adsorption. This highlights the significance of pH modification in real-world water treatment applications employing this composite material, as the ideal pH for Cr (VI) removal using these hydrogel beads usually lies in the acidic range.

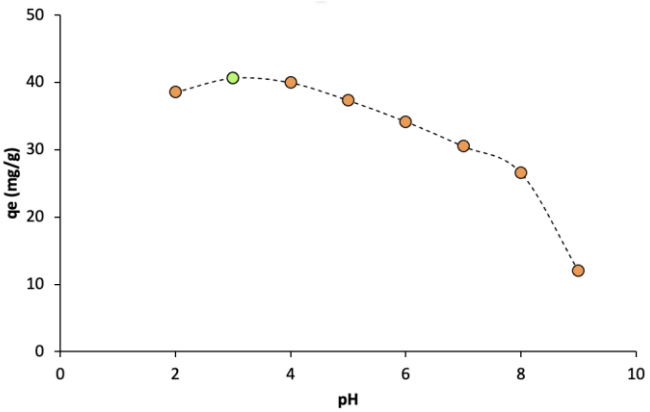

Figure 5. The effect of pH on Cr (VI) ions adsorption.

Effect of Cr (VI) Initial Concentration

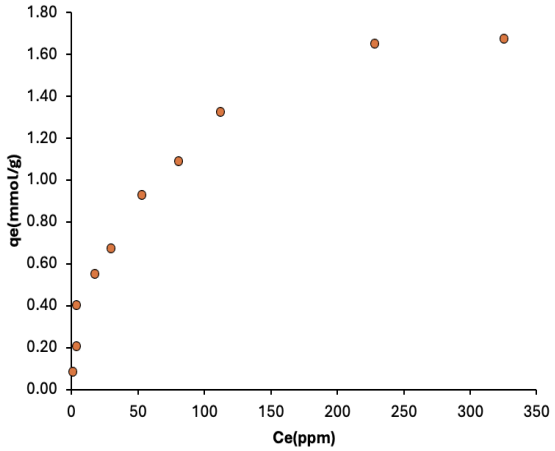

Figure 6. Effect of Cr (VI) ions concentration

An adsorption isotherm graph for removing Cr (VI) using nano-composite was given in the Figure 6. The graph, which plots the amount of Cr (VI) adsorbed (q_e) against its equilibrium concentration (Ce), shows a relationship typical of a monolayer adsorption process. The adsorption capacity was assessed by varying the Cr (VI) initial concentration (10, 25, 50, 75, 100, 150, 200, 250, 400 and 500 ppm). For $nTiO_2$–PKS–Cts@ECH, the adsorption was increased by enhancing the Cr (VI) concentration and could enhance the mass transfer between the liquid and solid phases to maximize the utilization of the active sites on the composite adsorbent. An increase in the Cr (VI) concentration enhanced the difference in adsorption capacity of the nano-composite. Initially, as the concentration of Cr (VI) increases, the amount adsorbed rises quickly. This steep increase indicates that the composite beads have a high affinity for Cr (VI) at low concentrations and that there are many available binding sites. Isotherm models are also important tools for understanding the mechanism of adsorption between the aqueous solution and the adsorbent. For this purpose, Langmuir, Freundlich, and D-R isotherm models were considered in the presented study. As the Cr (VI) concentration continues to increase, the rate of

adsorption slows down until the curve eventually flattens out. This plateau, or saturation point, signifies that most of the available active sites on the hydrogel beads are now occupied. At this point, the composite beads have reached its maximum adsorption capacity and can no longer effectively remove more Cr (VI) from the solution. This behavior is often characteristic of the Langmuir isotherm model, which suggests that the adsorption takes place on uniform sites on the adsorbent's surface (Chanajaree et al., 2021; Parlayıcı & Pehlivan, 2025). By applying the Langmuir model equation, the maximum Cr (VI) adsorption capacity of $nTiO_2$–PKS–Cts@ECH is 97.09 mg/g. Reduction, electrostatic interaction, and chemical adsorption together or some of them are active on the adsorption of the Cr (VI).

Table 1. Adsorption isotherm parameters for removal of Cr (VI) ions.

Model	Equation	Parameters for dye			
Langmuir	$\frac{C_e}{q_e} = \frac{C_e}{A_s} + \frac{1}{K_b A_s}$	**Q_m** 97.09	**K_b** 0.0255	**R^2** 0.985	**R_L** 0.282
Freundlich	$\ln q_e = \ln K_f + \frac{1}{n} \ln C_e$	**K_f** 6.001	**n** 1.99	**R^2** 0.924	
D-R	$\ln q_e = \ln q_m - \beta \varepsilon^2$	**X_m** 104.58	**K** 0.004	**E** 11.18	**R^2** 0.951

Effect of Contact Time and Kinetic Studies

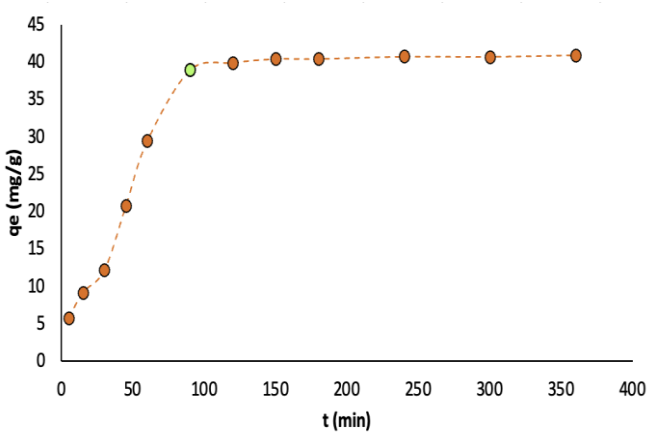

Figure 7. Effect of contact time on adsorption.

The effect of contact time on Cr (VI) adsorption was examined at different contact times (5, 15, 30, 45, 60, 90,120, 150, 180, 240, 300 and 360 min), 2.0 g/L adsorbent dosage, pH 3, 100 ppm Cr (VI) concentration, and 25 °C temperature to see how it affected the results. During the first 60 minutes, the adsorption process proceeds quickly, and the adsorption capacity increases significantly from about 6 mg/g to 29 mg/g. The time it took to attain equilibrium was influenced by the type of the adsorbent and the quantity of accessible active adsorption sites. The high number of easily accessible active sites on the composite beads' surface is what causes this quick early phase. After that, as the active sites are gradually occupied, the rate of adsorption starts to decrease. After around 90 minutes, the system starts to stabilize. The mass transfer resistance of the adsorbate from the bulk solution to the internal pores of the composite beads becomes the rate-limiting step as a result of this plateau, which shows that most of the accessible adsorption sites have been saturated.

Kinetic Models for Equlibrium

The adsorption kinetics curves for Cr (VI) removal by $nTiO_2$–PKS–Cts@ECH are shown in Figure 8. Table 2 presents the parameter results of both pseudo-first-order and pseudo-second-order kinetic models used to evaluate the adsorption data. The pseudo-second-order model provided a superior fit to the experimental results compared to the pseudo-first-order model. This is confirmed by the higher correlation coefficient (R^2) obtained for the pseudo-second-order model. Consequently, the adsorption process is more accurately explained by pseudo-second-order kinetics, indicating that chemisorption and electrostatic atraction is likely the dominant mechanism (Yuan & Lu, 2024).

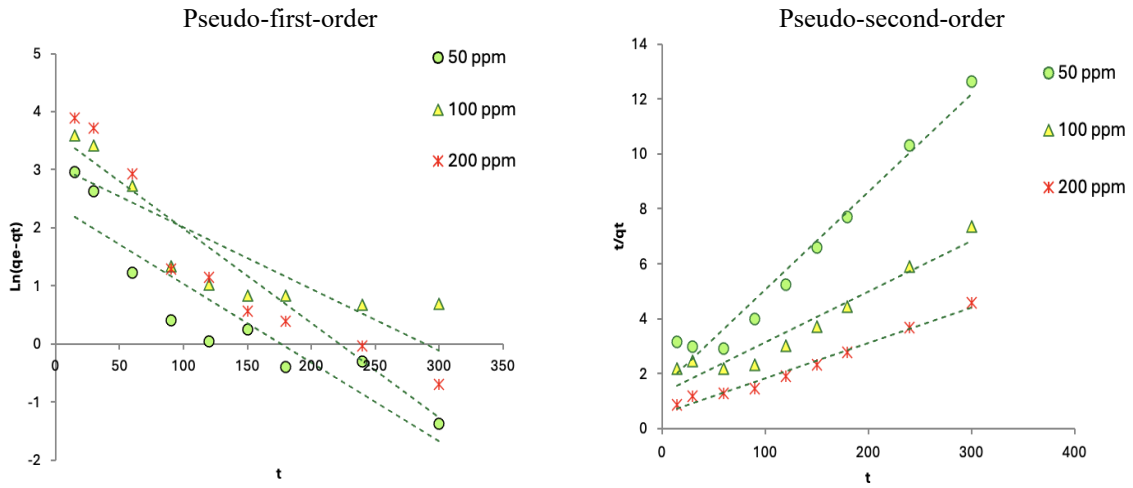

Figure 8. Kinetics for Cr (VI) ions adsorption onto nTiO₂–PKS–Cts@ECH composite.

Table 2. Comparison of the pseudo-first-order, pseudo-second-order adsorption rate constants and calculated and experimental q_e values obtained at different initial Cr (VI) concentrations.

		Pseudo-first-order			Pseudo-second-order		
C_o(ppm)	q_e exp	k_1	q_e	R^2	k_2	q_e	R^2
50	23.990	0.014	10.85	0.829	0.0009	28.01	0.968
100	42.775	0.011	21.69	0.709	0.0003	54.05	0.929
200	66.147	0.016	36.92	0.884	0.0003	77.52	0.981

Thermodynamic Studies

The effect of temperature on the adsorption of Cr (VI) onto nTiO₂–PKS–Cts@ECH was investigated (Figure 9), and the thermodynamic constants are given in Table 3. Negative ΔS° values reflect a decreased degree of disorder at the adsorbent-Cr (VI) interface in the solution phase during Cr (VI) adsorption onto the nTiO₂–PKS–Cts@ECH surface. A negative ΔH° value for Cr (VI) indicates that the adsorption of Cr (VI) onto nTiO₂–PKS–Cts@ECH is an exothermic process. Negative ΔG° values indicated that the adsorption of Cr (VI) onto nTiO₂–PKS–Cts@ECH is thermodynamically spontaneous and natural (Akiode et al., 2023). Additionally, the increase in ΔG° with increasing temperature indicates that the Cr (VI) adsorption process becomes more favorable at lower temperatures.

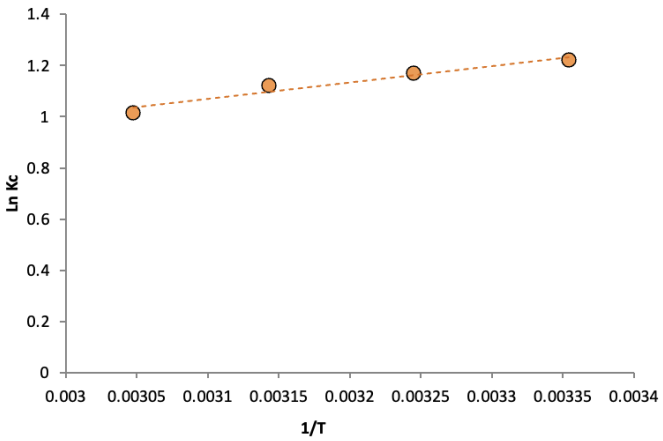

Figure 9. The impact of temperature on Cr (VI) adsorption.

Table 3. Thermodynamic parameters for adsorption of Cr (VI)

ΔS°	**ΔH°**	**ΔG° (J mol^{-1})**				
(J K^{-1}mol^{-1})	J mol^{-1}	T=298.15K	T=308.15K	T=318.15K	T=328.15K	R^2
-7.590	-5327.81	-3064.76	-2988.86	-2912.96	-2837.05	0.944

Conclusion

The $nTiO_2$–PKS–Cts@ECH nano-composite beads demonstrated considerable promise as a sustainable and highly efficient biosorbent for the removal of Cr (VI) from aqueous systems. Synthesized through the sol–gel method and stabilized via epichlorohydrin cross-linking, these nano-composite beads exhibited adsorption performance strongly influenced by operational factors such as solution pH, adsorbent dosage, contact duration, and the initial Cr (VI) concentration. Equilibrium analysis revealed that the Langmuir isotherm provided the best fit, consistent with a monolayer adsorption mechanism and yielding a maximum adsorption capacity of 97.09 mg/g. Kinetic modeling indicated a pseudo-second-order process, highlighting chemisorption, electrostatic interactions, and reduction as the governing mechanisms. Optimal removal occurred under acidic conditions, where protonated bead surfaces facilitated the uptake of dominant Cr (VI) species ($HCrO_4^-$ and $Cr_2O_7^{2-}$). Thermodynamic parameters confirmed that adsorption was spontaneous and exothermic, though less favorable at elevated temperatures. SEM imaging further illustrated that the porous structure of the hydrogel became saturated following Cr (VI) uptake. The results indicate that $nTiO_2$–PKS–Cts@ECH is a highly promising material for cleaning polluted water sources, specifically for removing Cr (VI).

Scientific Ethics Declaration

* The authors declare that the scientific ethical and legal responsibility of this article published in EPSTEM journal belongs to the authors.

Conflict of Interest

* The authors declare that they have no conflicts of interest

Funding

* This research received no specific grant from any funding agency in the public, commercial, or not-for-profit sectors.

Acknowledgements or Notes

* This article was presented as an oral presentation at the International Conference on Basic Sciences and Technology (www.icbast.net) held in Budapest/Hungary on August 28-31, 2025.

References

Akiode, O. K., Adetoro, A., Anene, A. I., Afolabi, S. O., & Alli, Y. A. (2023). Methodical study of chromium (VI) ion adsorption from aqueous solution using low-cost agro-waste material: Isotherm, kinetic, and thermodynamic studies. *Environmental Science and Pollution Research*, *30*(16), 48036-48047.

Al-Obaidi, N. S., Sadeq, Z. E., Mahmoud, Z. H., Abd, A. N., Al-Mahdawi, A. S., & Ali, F. K. (2023). Synthesis of chitosan-TiO2 nanocomposite for efficient Cr (VI) removal from contaminated wastewater sorption kinetics, thermodynamics and mechanism. *Journal of Oleo Science*, *72*(3), 337-346.

Alsuhaibani, A. M., Alayyafi, A. A., Albedair, L. A., El-Desouky, M. G., & El-Bindary, A. A. (2024). Efficient fabrication of a composite sponge for Cr (VI) removal via citric acid cross-linking of metal-organic framework and chitosan: adsorption isotherm, kinetic studies, and optimization using Box-Behnken design. *Materials Today Sustainability*, *26*, 100732.

Billah, R. E. K., Shekhawat, A., Mansouri, S., Majdoubi, H., Agunaou, M., Soufiane, A., & Jugade, R. (2022). Adsorptive removal of Cr (VI) by chitosan-SiO2-TiO2 nanocomposite. *Environmental Nanotechnology, Monitoring & Management*, *18*, 100695.

Chanajaree, R., Sriuttha, M., Lee, V. S., & Wittayanarakul, K. (2021). Thermodynamics and kinetics of cationic/anionic dyes adsorption on cross-linked chitosan. *Journal of Molecular Liquids*, *322*, 114507.

Guo, J., Zhou, T., Guo, H., Ge, C., & Lu, J. (2025). Application of nano-TiO2@ adsorbent composites in the treatment of dye wastewater: A review. *Journal of Engineered Fibers and Fabrics*, *20*, 15589250251329450.

Jiménez-Gómez, C. P., & Cecilia, J. A. (2020). Chitosan: A natural biopolymer with a wide and varied range of applications. *Molecules*, *25*(17), 3981.

Ke, C. L., Deng, F. S., Chuang, C. Y., & Lin, C. H. (2021). Antimicrobial actions and applications of chitosan. *Polymers*, *13*(6), 904.

Khan, M. K., Abdulhameed, A. S., Alshahrani, H., & Algburi, S. (2024). Chitosan/functionalized fruit stones as a highly efficient adsorbent biomaterial for adsorption of brilliant green dye: Comprehensive characterization and statistical optimization. *International Journal of Biological Macromolecules*, *263*, 130465.

Mahmoud, M. E., Elsayed, S. M., Mahmoud, S. E. M., Aljedaani, R. O., & Salam, M. A. (2022). Recent advances in adsorptive removal and catalytic reduction of hexavalent chromium by metal–organic frameworks composites. *Journal of Molecular Liquids*, *347*, 118274.

Mahmoud, M. E., El-Said, G. F., Ibrahim, G. A., & Elnashar, A. A. (2024). Effective removal of hexavalent chromium from water by sustainable nano-scaled waste avocado seeds: Adsorption isotherm, thermodynamics, kinetics, and error function. *Biomass Conversion and Biorefinery*, *14*(13), 14725-14743.

Masuku, M., Nure, J. F., Atagana, H. I., Hlongwa, N., & Nkambule, T. T. (2024). Pinecone biochar for the Adsorption of chromium (VI) from wastewater: Kinetics, thermodynamics, and adsorbent regeneration. *Environmental Research*, *258*, 119423.

Nishad, V., Kumar, S., & Sastry, S. V. A. R. (2025). Kinetics, isotherms and thermodynamics studies of Cr (VI) removal using zero-valent iron nanoparticles synthesized from Aegle marmelos (Bael) plant extract. *Nanotechnology for Environmental Engineering*, *10*(3), 66.

Parlayıcı, S., & Pehlivan, E. (2024). Methylene blue removal using nano-TiO2/MWCNT/Chitosan hydrogel composite beads in aqueous medium. *Chemosphere*, *365*, 143244.

Parlayıcı, S., & Pehlivan, E. (2025). Highly efficient hexavalent chromium removal using nano-Fe3O4/pomegranate peel biochar/Alginate composite as an advanced biosorbent. *Turkish Journal of Analytical Chemistry*, *7*(1), 22-32.

Rocher, V., Bee, A., Siaugue, J. M., & Cabuil, V. (2010). Dye removal from aqueous solution by magnetic alginate beads crosslinked with epichlorohydrin. *Journal of Hazardous Materials*, *178*(1-3), 434-439.

Teshome, S., Kassahun, S. K., & Tiruneh, S. N. (2024). Response surface statistical modeling for optimization of methylene blue adsorption from aqueous solution using chitosan/graphite composites: Isotherm and kinetics studies. *Separation Science and Technology*, *59*(2), 205-223.

Usmonova, Z., & Salixanova, D. (2025). Plum fruit peel as a raw material for obtaining activated carbon adsorbents. In *AIP Conference Proceedings* (Vol. 3304, No. 1, p. 040029). AIP Publishing LLC.

Yuan, J., & Lu, W. (2024). Adsorption of Cr (VI) from aqueous solutions using inorganic clays modified magnetic chitosan adsorbent: Kinetic and thermodynamic study. *Desalination and Water Treatment*, *319*, 100442.

Zewde, Z., Asere, T. G., & Yitbarek, M. (2024). Porous biochars derived from brewery waste for the treatment of Cr (VI)-contaminated water. *PLoS One*, *19*(11), e0314522.

Author(s) Information

Serife Parlayici
Konya Technical University, Faculty of Engineering and Natural Sciences, Department of Chemical Engineering, Rauf Orbay Street. 42250, Selçuklu/Konya, Türkiye

Erol Pehlivan
Konya Technical University, Faculty of Engineering and Natural Sciences Department of Chemical Engineering Rauf Orbay Street. 42250, Selçuklu/Konya, Türkiye
Contact e-mail: *erolpehlivan@gmail.com*

To cite this article:

Parlayici, S. & Pehlivan E. (2025). Epichlorohydrin-crosslinked nano-TiO_2/plum kernel shell/chitosan hydrogel beads for the efficient removal of hexavalent chromium from aqueous solutions *The Eurasia Proceedings of Science, Technology, Engineering and Mathematics (EPSTEM), 36,* 1-10.